INTERNATIONAL JOURNAL OF CHEMICAL REACTOR ENGINEERING

Volume 3 2005 *Article* A50

Modelling a Biochemical Reaction with Computational Fluid Dynamics

Sotos C. Generalis* Gregory M. Cartland Glover†

*Aston University, S.C.Generalis@aston.ac.uk

†Forschungzentrum Rossendorf, Institute for Safety Research, Germany, g.glover@fz-rossendorf.de

ISSN 1542-6580

Modelling a Biochemical Reaction with Computational Fluid Dynamics

Sotos C. Generalis and Gregory M. Cartland Glover

Abstract

Earlier investigations (Cartland Glover et al., 2004) into the use of computational fluid dynamics (CFD) for the modelling of gas-liquid and gas-liquid-solid flow allowed a simple biochemical reaction model to be implemented. A single plane mesh was used to represent the transport and reaction of molasses, the mould Aspergillus niger and citric acid in a bubble column with a height to diameter aspect ratio of 20:1. Two specific growth rates were used to examine the impact that biomass growth had on the local solids concentration and the effect this had on the local hydrodynamics of the bubble column.

KEYWORDS: gas-liquid-solid flows, bubble columns reactors, computational fluid dynamics, fermentation, mixture model

1. INTRODUCTION

A good example of a biochemical reaction that could be employed in gas-liquid-solid flow simulations with CFD is the fermentation of sugars to form citric acid. In the 80 years since citric acid was first commercially manufactured many process routes have been developed that can be grouped into either surface or submerged cell cultures (Atkinson and Mavituna, 1983; Bailey and Ollis, 1986; Chisti, 1989; Deckwer, 1986; Finkelsein and Ball, 1991). Surface cultures consist of warm air blown over shallow pans of inoculated media and submerged cultures generally occur in stirred tank or airlift reactors where the gas phase agitates and oxygenates the solid and liquid phases.

A large number of fungal organisms are known to excrete citric acid including various species of the moulds *Aspergillus*, *Penicillium* and *Candida*. The mould known as *Aspergillus niger* is widely preferred for the manufacture of citric acid in the submerged cultures (Atkinson and Mavituna, 1983). The broth composition and the conditions applied to the fermentation have a direct influence on the cell growth (Atkinson and Mavituna, 1983; Bailey and Ollis, 1986; Berovič et al., 1993; Chisti, 1989; ; Coulson et al., 1994; Deckwer, 1986; Finkelsein and Ball, 1991; Haq et al., 2002; Roehr et al., 1981; Sakurai et al., 1997; Sankpal et al., 2001). Particularly as fungal moulds are vegetative organisms that grow aerobically and obtain their energy by oxidising organic substances (Coulson et al., 1994). The product formed by the fungal mould is usually a result of metabolic processes within the organism (Coulson et al., 1994). Several metabolic pathways control the development of cells; however the local environmental conditions (i.e. broth composition, oxygen concentration, pH and temperature) determine the pathway that is employed by the microbes to grow, thus influencing the products formed and the rates of growth (Atkinson and Mavituna, 1983; Bailey and Ollis, 1986; Berovič et al., 1993; Haq et al., 2002; Roehr et al., 1981; Sakurai et al., 1997; Sankpal et al., 2001).

The time scale of fermentations is measured in days as the life cycle of the culture is spread over stages of non-growth, accelerated growth and product formation that take many hours to complete (Roehr et al., 1981). The conditions that promote cell growth and ultimately product formation requires the broth or medium composition to be a complex mixture of carbohydrates, sources of nitrogen, phosphorous and sulphur. Carbohydrates provide energy and material for the formation of metabolic products (including the growth of cells) and as a result of which the form of carbohydrate is usually pure glucose, starch or sucrose. The energy and materials for metabolic processes can also be derived from raw starch, sugar or molasses. Other forms of carbohydrates include waste vegetable matter, such as fruit peels or mashes. The sources of nitrogen, phosphorous and sulphur are provided in the form of inorganic salts of ammonium, magnesium and potassium. Other factors that affect the production of citric acid using *Aspergillus niger* include the pH of the broth (1.5-2.8), the temperature (28-33°C) and length of the fermentation of the order of 6 to 25 days (Atkinson and Mavituna, 1983; Finkelsein and Ball, 1991).

It is important to note that how the culture develops is heavily dependent on the trace metals and the anionic complexes that are added to the broth with the carbohydrate sources. Trace metals used in broths include copper, iron, manganese and zinc where the concentration of each metal has a bearing on the growth and product formation rates. Too much iron or too little copper in the broth could cause formation of various types of pellet or even a viscous mixture (Atkinson and Mavituna, 1983; Haq et al., 2002). Note that the most effective form the cell culture is grown as loose fluffy pellets, as the mass transfer rates across phase boundaries (gas-liquid and liquid-pellet) are greater for these cultures.

A great deal of effort has been invested in understanding how citric acid is formed by micro-organisms at scales that range from the single cell (>5μm) up to process scale bio-reactors, which can be up to several metres in diameter (Atkinson and Mavituna, 1983; Finkelsein and Ball, 1991). Therefore, it is still difficult to understand many of the reactions that take place in fermentation processes, as observation of the reactions *in situ* is difficult. The impact that the environmental factors have on growth of a fungal mould during each stage of fermentation increase the complexity of the design and operational procedures for biochemical reactors. This is apparent when each individual cell acts in a different manner due the age of the cell and changes in the local environment for the entire fermentation i.e. local substrate concentrations plus the presence of nitrates, sulphates and specific trace metals (Atkinson and Mavituna,

1983; Haq et al., 2002; Roehr et al., 1981; Sakurai et al., 1997; Sankpal et al., 2001). CFD can help improve understanding of the influence that changes in the local environment have on the cell culture and the formation of extracellular products such as citric acid at different stages of the culture life cycle.

The modelling of a biochemical reaction with CFD can be treated in many ways from the simple to the very complex. The complex models involve mimicking the metabolic pathways for product synthesis in a single cell, observing how simple changes to the environmental conditions influence the pathways that are utilized (Alvarez-Vasquez et al., 2000). As reactions in a single cell are highly non-linear, power law models were employed to model each of the component reactions and therefore enable the prediction of chemical reactions under specific conditions (Alvarez-Vasquez et al., 2000). But single cell representations of the culture are far too complex for implementing with the continuum representation of multiphase flow models employed in CFD. Therefore it would be prudent to consider a volume-averaged approach, such as those applied to diffusion and reaction in a bio-film of pellets that were formed by cell growth (Kissel et al., 1984; Rittmann et al., 1984; Wanner and Gujer, 1986; Wood and Whitaker, 1998).

The definition of the volume-averaged model that is employed in predicting biochemical reactions is dependent on the scale at which the biofilm is regarded. Six levels of different length scales can be considered from the aquifer level for trickling filters that are commonly used in water treatment to length scales associated with microbes such as the membrane thickness, length, width (Wood and Whitaker, 1998). The focus of the derived models (Wood and Whitaker, 1998) through the volume averaging of length scales associated with the biofilm thickness and a two-phase system of that consisted of microbes and a polysaccharide matrix that forms the biofilm structure. The scales considered were far below that of the macroscopic flow structures described by the multiphase flow methods (Cartland Glover et al., 2004A-B). Therefore, the implementation of models that include the transport and reaction of mass on a larger scale were considered (Kissel et al., 1984; Rittmann and McCarthy, 1980; Wanner and Gujer, 1986). For reasons of simplifying the models derived (Kissel et al., 1984; Rittmann and McCarthy, 1980; Wanner and Gujer, 1986) the biofilm was considered as a single continuum phase where reaction and diffusion occurred throughout the film and not just in the microbes. This increased the length scale at which the diffusion coefficients were calculated, ignoring the effects of the geometry of the microbes and the surrounding environment even though competing organisms were considered in the treatment of the models (Kissel et al., 1984; Wanner and Gujer, 1986).

Recently a model (Sakurai et al. 1997) presented that calculated the production of citric acid by fermenting sugars in the presence of *Aspergillus niger* using a rotating disc contactor. Employing experimentally derived reaction rates and yield coefficients and solved the mass balances numerically and provided a good comparison with changes in cell mass, product and substrate concentrations (Sakurai et al. 1997). The model expressed cell growth and product formation in terms of Monod and Luedeking-Piret rate equations Bailey and Ollis, 1986; Coulson et al., 1994; Deckwer, 1986; Sinclair and Kristiansen, 1987). Inter-phase oxygen transport was considered along with the transport of sugars, as oxygen is a limiting substrate in the growth and maintenance metabolic pathways of which citric acid is a by-product (Coulson et al., 1994; Sakurai et al., 1997). This introduces many difficulties into the modelling of gas-liquid-solid flows using CFD, with changes in the molecular weight and density of the gas phase. The transfer of oxygen influences the pressure acting on the bubbles and would therefore influence the size and shape of the bubbles. The biofilm in the rotating disc contactor where the biofilm is supported by a disc, this differs from the biofilms that occur in a bubble column where the biomass has the form of pellets or a viscous broth (Finkelstein and Ball, 1991; Sakurai et al., 1997). Therefore the boundary conditions applied to the species transport and reaction models were reconsidered before their implementation into the reaction models.

2. METHOD

2.1 Transport Equations

The equations that describe the flow phenomena for multiphase flow and reaction are given by Equations (1)-(7). The continuity and momentum equations, Equations (1)-(2), and scalar transport

equations, Equations (4)-(7), model the transport of each phase and each species through the domains considered. The influence of turbulent flow interactions is modelled by the exact Reynolds stresses, Equation (8), that was found to give an accurate representation of the velocity field for gas-liquid flow (Cartland Glover et al., 2004A). The solver (Fluent Inc., 1998) employed Equation (8) as a series of equations that enable the closure of the unknown terms (Cartland Glover et al., 2004A).

$$\frac{\partial}{\partial t}\left(\rho_{mp}\right)+\frac{\partial}{\partial x_i}\left(\rho_{mp}u_{mp,i}\right)=S_s \tag{1}$$

$$\frac{\partial}{\partial t}\left(\rho_{mp}u_{mp,i}\right)+\frac{\partial}{\partial x_i}\left(\rho_{mp}u_{mp,i}u_{mp,j}\right)=-\frac{\partial p}{\partial x_j}+\rho_{mp}g_j+F_j+\frac{\partial}{\partial x_i}\sum_{q=1}^{n}\phi'_q\rho_q u_{Dq,i}u_{Dq,j} + \frac{\partial}{\partial x_i}\mu_{eff}\left(\frac{\partial}{\partial x_j}\left(u_{mp,i}\right)+\frac{\partial}{\partial x_i}\left(u_{mp,j}\right)\right) \tag{2}$$

$$\frac{\partial\phi'_G}{\partial t}+\frac{\partial}{\partial x_i}\left(\rho u_{mp,i}\phi'_G-\Gamma_{\phi'}\frac{\partial\phi'_G}{\partial x_i}\right)=\nabla\left(\phi'_G\rho_G u_{mp,i}+\sum_{G=1}^{n}\phi'_G\rho_G u_{DG,i}\right) + \nabla\left(\mu_{eff}\left(\frac{\partial}{\partial x_j}\left(u_{mp,i}\right)+\frac{\partial}{\partial x_i}\left(u_{mp,j}\right)\right)\right) \tag{3}$$

$$\frac{\partial\phi'_S}{\partial t}+\frac{\partial}{\partial x_i}\left(\rho u_{mp,i}\phi'_S-\Gamma_{\phi'}\frac{\partial\phi'_S}{\partial x_i}\right)=\phi'_{SG}+\nabla\left(\phi'_S\rho_S u_{mp,i}+\sum_{S=1}^{n}\phi'_S\rho_S u_{DS,i}\right) + \nabla\left(\mu_{eff}\left(\frac{\partial}{\partial x_j}\left(u_{mp,i}\right)+\frac{\partial}{\partial x_i}\left(u_{mp,j}\right)\right)\right) \tag{4}$$

$$\frac{\partial\phi''_B}{\partial t}+\frac{\partial}{\partial x_i}\left(\rho u_{mp,i}\phi''_B-\Gamma_{\phi''_B}\frac{\partial\phi''_B}{\partial x_i}\right)=\lambda\rho_L\phi''_B \tag{5}$$

$$\frac{\partial\phi''_A}{\partial t}+\frac{\partial}{\partial x_i}\left(\rho u_{mp,i}\phi''_A-\Gamma_{\phi''_A}\frac{\partial\phi''_A}{\partial x_i}\right)=-\left(\frac{1}{Y_{B/A}}+\frac{Y_{C/B}}{Y_{C/A}}\right)\lambda\rho_L\phi''_B \tag{6}$$

$$\frac{\partial\phi''_C}{\partial t}+\frac{\partial}{\partial x_i}\left(\rho u_{mp,i}\phi''_C-\Gamma_{\phi''_C}\frac{\partial\phi''_C}{\partial x_i}\right)=Y_{C/B}\lambda\rho_L\phi''_B \tag{7}$$

$$\frac{\partial}{\partial t}\left(\rho\overline{u_iu_j}\right)+\frac{\partial}{\partial x_l}\left(\rho U_l\overline{u_iu_j}\right)=-\frac{\partial}{\partial x_l}\left[\rho\overline{u_iu_ju_l}+\overline{p\left(\delta_{lj}u_i+\delta_{il}u_j\right)}\right]+\frac{\partial}{\partial x_l}\left[\mu\frac{\partial}{\partial x_l}\left(\overline{u_iu_j}\right)\right] - \rho\left(\overline{u_iu_l}\frac{\partial U_j}{\partial x_l}+\overline{u_ju_l}\frac{\partial U_i}{\partial x_l}\right)+p\left(\frac{\partial u_i}{\partial x_j}+\frac{\partial u_j}{\partial x_i}\right)-\rho\beta\left(g_i\overline{u_j\theta}+g_j\overline{u_i\theta}\right) - 2\mu\overline{\frac{\partial u_i}{\partial x_l}\frac{\partial u_j}{\partial x_l}}-2\rho\Omega_l\left(\overline{u_ju_m\varepsilon_{ikm}}+\overline{u_iu_m\varepsilon_{jkm}}\right) \tag{8}$$

2.2 Species transport and reaction models

Generic reaction models were derived that depicted the growth of the biomass through the consumption of a substrate (molasses) and the formation of an extracellular product to represent citric acid (Sinclair and Kristiansen, 1987). Three equations for the change in the concentration of the biomass in Equation (4), substrate in Equation (5) and product in Equation (6) were obtained. Note that the diffusion coefficients for each of the concentration equations defining the transport of the chemical species were defined as 10^{-3}. Yield coefficients were then applied to the cell growth rate term ((rhs) of Equation (5)) to determine the substrate consumption rate with respect to cell growth and product formation (rhs of Equation (6)). The rate of product formation is also related to the cell growth rate and the resultant term (rhs of Equation (7)) is used to predict the mass of substrate consumed by the formation of the product. The scalar equations that model the transport of the cell culture and the chemical species are similar to the equations for a bioreactor (Sakurai et al., 1997; Sinclair and Kristiansen, 1987). The differences between the equations based on the whole reactor and Equations (3) to (7) are the terms on the left hand side of the equation that model the convection and diffusion of the species across the reactor and that the cell culture is treated as a volume fraction. Therefore all that is needed to model the growth of the cell culture is an additional source term in the volume fraction equation for the solid phase.

To account for the effect of biomass growth on the local solid phase fraction an extra source term (first term on the rhs of Equation (4)) was used to calculate the increase in the volume fraction of the solid phase that is caused by the growth of cells. Note that the reaction models are dimensionless and need conversion to units of concentration before conversion of the biomass grown to a volume fraction, by the use of Equations (9)-(12).

$$V_L = \left(1 - \left(\phi'_G + \phi'_S\right)\right)V_{CC} \tag{9}$$

$$M_B = \lambda \rho_L \phi''_B V_L \tag{10}$$

$$V_B = M_B / \rho_S \tag{11}$$

$$\phi'_{SG} = \frac{V_B}{V_{CC}} \tag{12}.$$

The following assumptions were made for the use of the reaction models:

- the reaction and transport of chemical species occur in a batch reactor
- all reactions and phase interactions are isothermal
- pseudo-steady state conditions apply to the biofilm
- the cell culture is a suspension of loose pellets where initially one fifth of the solids present are biologically viable
- a single substrate is consumed as a result of the cell growth and maintenance mechanisms
- one extra-cellular product species is formed as a result of cell growth and maintenance metabolisms
- no transport of oxygen across the gas, liquid or solid phase interfaces
- cell growth and maintenance rates are combined into one rate and is expressed as a specific growth rate
- when the concentration of the substrate reaches zero, both the substrate consumption, cell growth and product formation rates become zero
- the substrate and the product are assumed to have a negligible effect on the mixture viscosity

2.3 Multiphase flow models

The multiphase model employed was the mixture model that was based on the drift flux model (Ishii and Mishima, 1984; Maninnien et al., 1996; Sanyal et al., 1999; Zuber and Findlay, 1965; Zuber and Ishii, 1979). The continuous and discrete phases are treated as a pseudo-continuous mixture that is modelled by the continuity (1) and momentum (2) equations supplemented by the mixture density equation, Equation (13), and the mixture viscosity of Equation (14)-(16). To predict the volume fraction of the gas and solid phases and their motion through a bubble column, two scalar equations, Equations ((3) and (4)), were employed in conjunction with Equations (1) and (2).

In order to capture the transport of the discrete phase additional source terms were applied to Equations (3) and (4). The last term on the right hand side of Equations (3) and (4) is the deviatoric stress tensor and the second to last term is the inter-phase interaction term as calculated by the drift velocity. The first term on the right hand side of Equation (3) and the second term on the right hand side of Equation (4) is the convective flux of the respective discrete phase. We note that there are two convective fluxes with one representing the effect of mixture phase in each volume fraction equation. The third term on the lhs of Equations (3) and (4) model the diffusion of the phases, and the coefficients of that term were defined as 0.1 for each discrete phase.

The term that introduces the drift velocity interaction is on the right hand side of Equations (2)-(4). This was calculated by employing velocity formulations of the mass-averaged velocity, Equation (17), the drift velocity, Equation (18) and the slip velocity Equation (19). The friction factor in Equation (19) was calculated by using Equation (20), which is dependent on the particle Reynolds number defined in Equation (21). Equations (13)-(21) are given as follows:

$$\rho_{mp} = \sum_{q=1}^{n} \phi'_q \rho_q \tag{13}$$

$$\mu_{mp} = \mu_c \left(1 - \frac{\phi'}{\phi'_{qm}} \right)^{-2.5 \phi'_{qm} \mu^*} \tag{14}$$

$$\mu^* = 1 \tag{15}$$

$$\mu^* = \frac{\mu_q + 0.4\,\mu_c}{\mu_q + \mu_c} \tag{16}$$

$$\vec{u}_{mp} = \frac{\sum_{q=1}^{n} \phi'_q \rho_q \vec{u}_q}{\rho_{mp}} \tag{17}$$

$$\vec{u}_{Dq} = \vec{u}_q - \vec{u}_{mp} = \vec{v}_{q,c} - \frac{1}{\rho_{mp}} \sum_{r=1}^{n-1} \phi'_r \rho_r \vec{v}_{r,c} \tag{18}$$

$$\vec{v}_{q,c} = \vec{u}_q - \vec{u}_c = \frac{d_q^2 \left(\rho_{mp} - \rho_q \right)}{18 \mu_c f} \left(g_j - \frac{D\vec{u}_{mp}}{Dt} \right) \tag{19}$$

$$f = 1 + 0.05\, Re^{0.687} \qquad Re < 1000 \tag{20a}$$

$$f = 0.018\,Re \qquad Re \geq 1000 \tag{20b}$$

$$Re = \frac{d_q u_{mp} \rho_c}{\mu_c} \tag{21}$$

2.4 Boundary conditions

The domain is defined as a two-dimensional plane mesh with a height to width aspect ratio of 20:1. The mesh was a 4500 computational cell domain with 300 mesh cells in the vertical direction and 15 mesh cells in the horizontal direction. This mesh corresponded to an experimental rig that was used to investigate the morphological and rheological properties of an *Aspergillus niger* fermentation in a bubble column (Berovič et al., 1993). The dimensions of each mesh cell for both flow domains were 0.01 × 0.01 m with respect to the horizontal and vertical directions.

Solving the gas-liquid-solid flow field for a large aspect ratio meshes is useful in understanding how the flow characteristics of bubble column and airlift fermentation reactors change with column height. Generally large aspect ratio columns are employed for submerged culture fermentations as the greater hydrostatic head increases the transfer of oxygen from the gas phase to the liquid phase (Finkelstein and Ball, 1991). Oxygen is critical to many fermentation processes as the organism employed requires dissolved oxygen to convert carbohydrates into energy and materials for metabolic products (Atkinson and Mavituna, 1983; Bailey and Ollis, 1986; Coulson et al., 1994; Finkelstein and Ball, 1991).

Velocity inlet conditions are applied to the base of both meshes, with the volume fraction and vertical velocity of the gas phase defined as a flux. The inlet for the 20:1 mesh employed the whole of the bottom surface of the domain. The top boundary was defined as a pressure inlet that was applied to the whole of the top surface. The remaining boundaries were treated as walls, where no species fluxes were defined i.e. the discrete phase or the solutes were specified as zero and without gradients. These specifications were also applied to the bottom and top surfaces for the solid, biomass, substrate and product species. Only the gas phase was treated differently. The gas enters through the bottom surface and leaves the domain through the top surface as a flux.

2.5 Physical properties

In solving the reaction models that were applied to the biomass, substrate and product species experimental rates of reaction and yield coefficients were required to relate the physical phenomena occurring in a fermentation process to the influence of the computational flow field. Experimentally derived reaction rates for cell growth, substrate consumption and product formation for two strains of the *Aspergillus niger* species of mould were assessed from a study of the fermentation of each species in a chemostat (Haq et al., 2002). However, the models derived ignored the influence of oxygen on the biomass.

The concentration of copper ions was varied with the addition of the carbonate, chloride, nitrate or sulphate salts of copper (Haq et al., 2002). Observable differences in cell growth and morphology resulted in changes to the rate at which the molasses were consumed and the product that was formed. When $2*10^{-5}$ M of copper sulphate was added to the fermentation medium, an increase of 20 % of the yield of citric acid was observed. The addition of copper sulphate promoted the formation of pellets that were loose and fluffy resulting in improved mass transfer rates. This led to increases in citric acid production rate with little significant increase in the carbohydrate consumption rate. Growth rates and the yield coefficients of sugar consumption and citric acid formation for the controlled fermentations of a wild and modified strain were presented. For the fermentations $2*10^{-5}$ M of copper sulphate was added. The reported growth rates used in the simulations here included a wild and a modified strain of *A. niger*, which can be found in Table 1.

Table 1. Kinetic and stoichiometric parameters applied to the biochemical reaction model (Haq et al., 2002)

Parameter	Units	A	B
Specific Growth Rate	s^{-1}	$6.5*10^{-5}$	$1.522*10^{-4}$
Yield of cells per unit substrate consumed	kg cells (kg substrate)$^{-1}$	0.118	0.148
Yield of product per unit substrate consumed	kg product (kg substrate)$^{-1}$	0.442	1.087
Yield of product per unit mass of cells	kg product (kg cells)$^{-1}$	3.572	7.360

The physical properties of the gas, liquid and solid phases that are represented in this model include the density, the particle size and the viscosity of each phase. The density and viscosity of the fluid phases are defined as 1.225 kg m^{-3} and $1.7894*10^{-5}$ kg m^{-1} s^{-1} for air, 998.2 kg m^{-3} and $1.003*10^{-3}$ kg m^{-1} s^{-1} for water. The density for the solid phase was 1080 kg m^{-3} with Equations (14) and (15) relating the impact that the solid phase had on the fluid viscosity. The particle diameter of the gas phase was defined as 5 mm and the solid phase particle diameter was 0.1mm, where the form of both types of particle was assumed to be spherical. The diameters were kept the same as the particle diameters from previous investigations for reasons of consistency. Additionally the particle diameter of the solid phase was assumed to be constant for whole length of the simulation. Therefore, it was assumed that there was no increase in the solid particle diameter, just an increase in the number of particles as the mass of cells increased.

2.6 Solution strategies

The discretization techniques and under-relaxation factors applied when modelling discrete phase transport remain unchanged from the gas-liquid flow cases (Cartland Glover et al., 2004A). We note that the discretization schemes and under-relaxation factors for both the discrete phases and the chemical species are specified in the same manner for reasons of consistency.

The fraction of the gas phase at the inlet at the bottom of the column was then defined as 0.6 and as a flux at a superficial gas velocity of 2 cm s^{-1}. This resulted in a velocity of 0.036 m s^{-1} being applied to the inlet condition. The volume fraction of the solid phase, biomass, substrate and product concentrations were initialised, respectively as 0.005, 0.001, 0.15 and 0 (equivalent to 5, 1, 150 and 0 kg m^{-3}) with the assumption of complete mixing giving uniform concentration distributions. The gas phase fraction and the velocity fields were initialised with a flow-field from a fully developed gas liquid flow. The local change in gas and solid phase fractions and the impact that this had on the local velocities and concentrations were then solved for 2000 time-steps or 200 seconds of flow time with a time-step size of 0.1 s.

3. RESULTS

The hydrodynamic modelling of gas-liquid flow with regards to the velocity profile has been previously validated for a bubble column with a 5:1 height to diameter aspect ratio (Cartland Glover, 2002; Cartland Glover and Generalis, 2004A). This model was then modified to include a plausible representation of the effect that the introduction of a particulate solid phase has on the gas-liquid motion (Cartland Glover and Generalis, 2004B). However, the application of the solid phase to the gas-liquid flow model was not explicitly validated due to a lack of experimental data on the distribution of the solid phase for the same system.

Further modifications to the gas-liquid-solid flow model included the use of a simple biochemical reaction model that was the applied to the same domain (Cartland Glover, 2002). These simulations were performed to observe the impact the transient hydrodynamics have on the transport of the substrate, product and biomass species (Cartland Glover, 2002). However, there was a strong absence of detailed hydrodynamic and biochemical reaction data that has been experimentally obtained with regard to the same operating conditions (i.e. bubble column geometry, gas flow rates, local hydrodynamic measurements) and measured biochemical reaction kinetics (rates of cell growth substrate consumption and product formation; local concentrations of the biomass, substrate and product) limited the scope for validation (Cartland Glover et al., 2005BC).

Therefore, an alternative bubble column geometry with a 20:1 height to diameter aspect ratio where experimental observations on the hydrodynamics with regard to the shear rate and the effect that this had on the biomass was selected (Berovič et al., 1993). Analysing the resultant flow phenomena that was determined by the simulations, it is possible to infer regions of high substrate consumption and product formation. This is possible through the use of times series (Figures. 1-2), profile (Figures. 3-4) and field plots (Figures. 5-8).

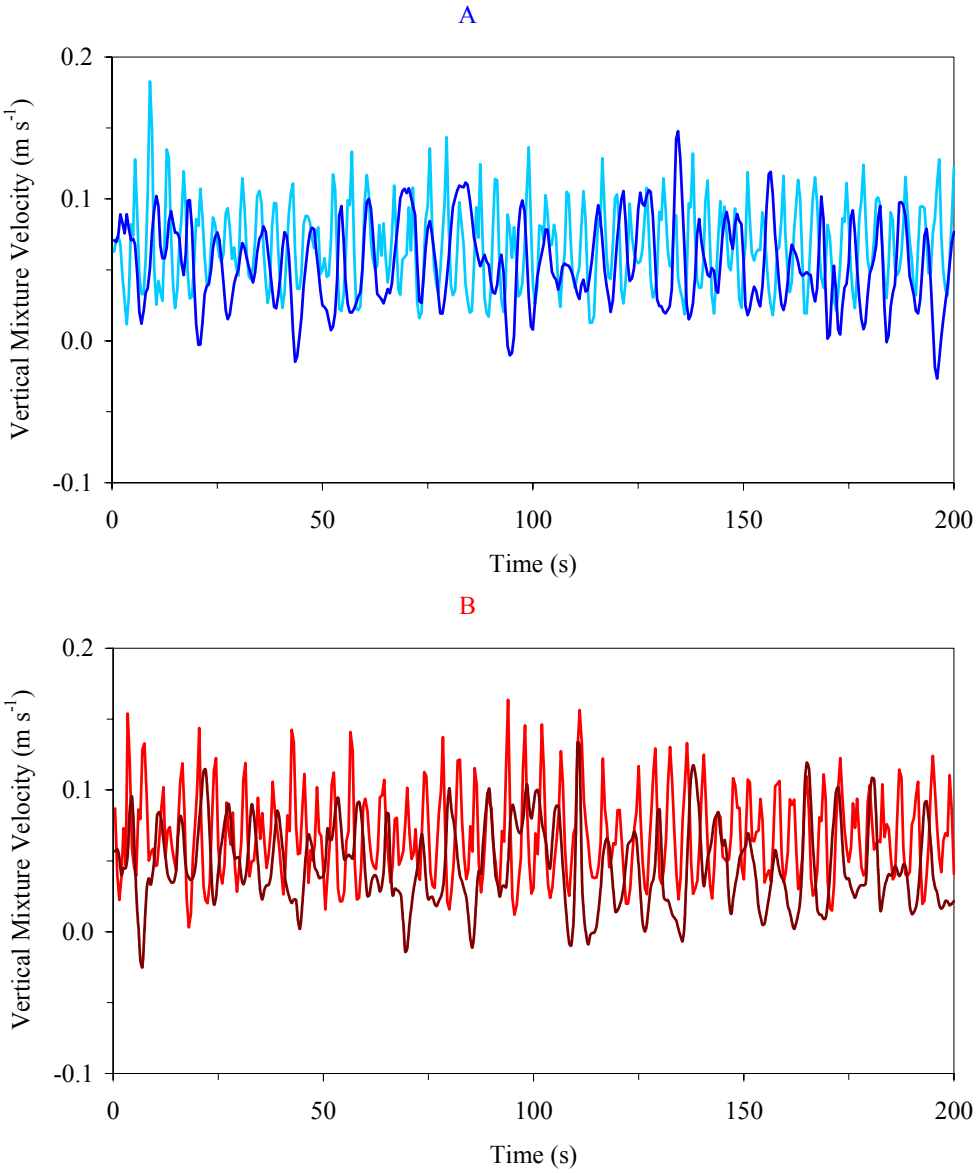

Figure 1. Time series for the vertical mixture velocity (m s^{-1}) for growth rates A and B; Brighter colours at a height of 2.5 column diameters and darker colours at a height of 10 column diameters;

The time series for the vertical mixture velocity for growth rates A and B are depicted in Figure 1 on the column centreline with one point at the midpoint of the column (i.e. at a height of 10 column diameters) and a second point location at a height of 2.5 column diameters. Both time series show an unstable flow; however, the fluctuation of in the velocity is less intense for both growth rates at the point located at 10 column diameters. The reason for the reduction in the intensity is that the point is significantly further away from the gas inlet, which is the source of the turbulence energy in these cases.

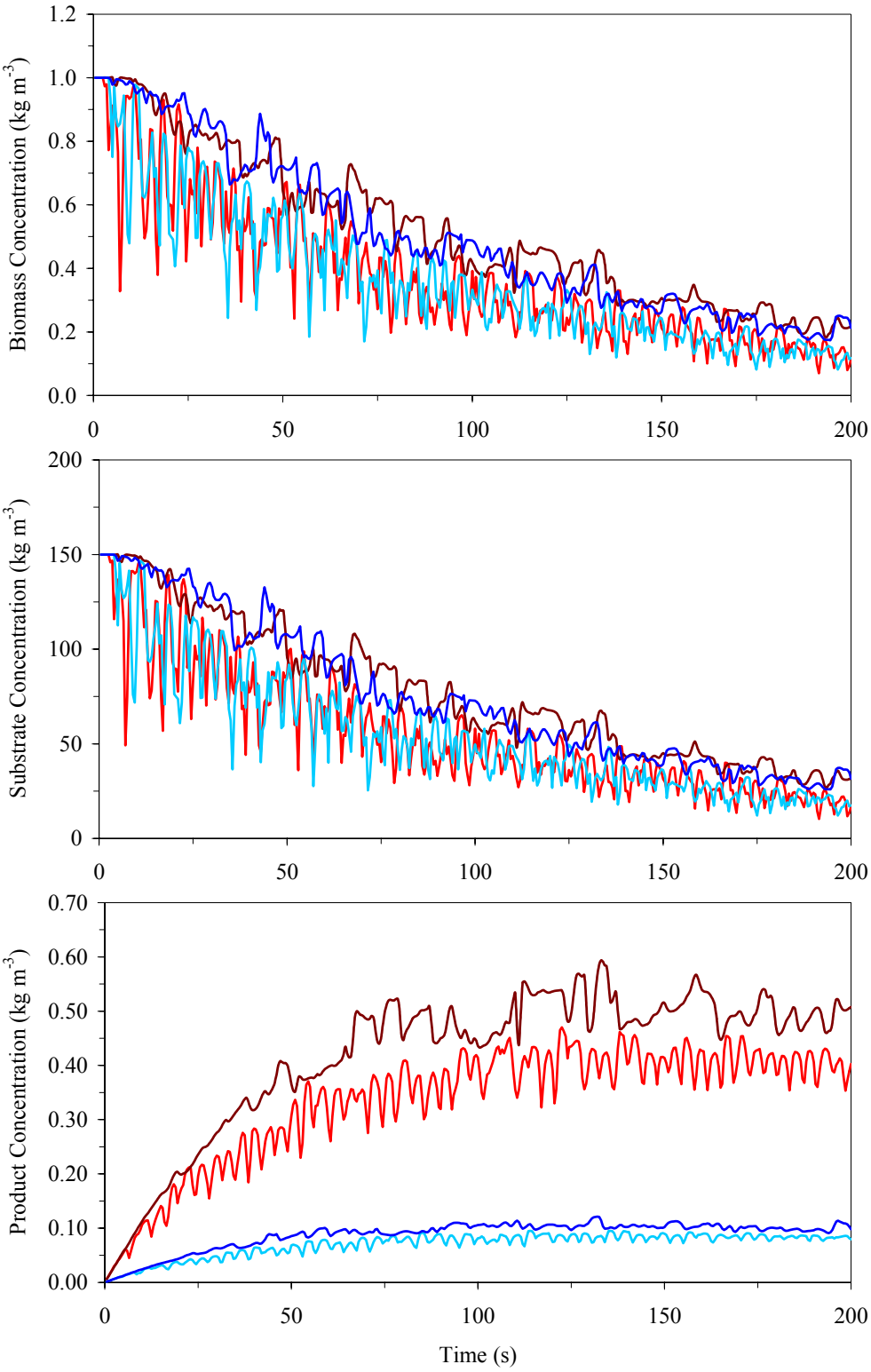

Figure 2. Time series for the biomass, substrate and product concentrations (kg m^{-3}) for growth rates A and B; Brighter colours at a height of 2.5 column diameters and darker colours at a height of 10 column diameters;

The series in Figure 2 present the concentrations for the biomass, substrate and product species. The change in the concentrations of the species can be described as power law functions. We also observed that the rates at which the substrate was consumed and the product was formed reduce in value as the concentration of the substrate species reduces. The influence of the turbulence caused by the injection of the gas phase decreases the further away from the gas phase inlet is demonstrated by the reduction in the fluctuations of all the time series. Generally the concentration of the three biochemical reaction components appears to be greater at a height of ten column diameters. However, the biomass concentration reduces at the selected points with time suggesting that biomass is lost from the system or collecting in one region.

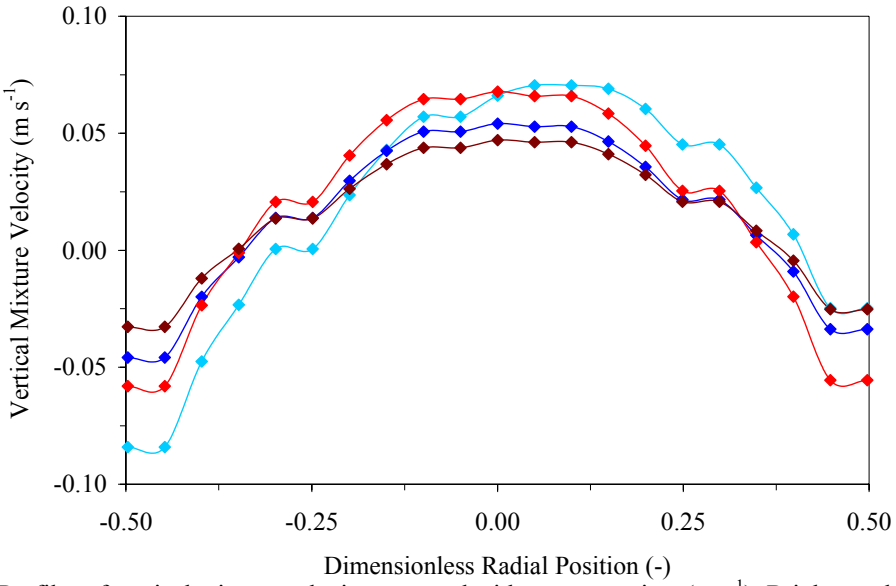

Figure 3. Profiles of vertical mixture velocity averaged with respect to time (m s^{-1}); Brighter colours at a height of 2.5 column diameters and darker colours at a height of 10 column diameters; Blue profiles for rate A and red profiles for rate B;

The profiles of the time-averaged vertical velocity of the mixture are found in Figure 3. All the profiles are parabolic. At half the 20:1 column's height the profile varies between 0.05 m s^{-1} at the column centre and -0.05 m s^{-1} at the column walls, whereas at a height of 2.5 column diameters the maximums are up to |0.09| m s^{-1}. Comparing the equivalent column diameter heights, i.e. at 2.5 column diameters for the 5:1 and 20:1 column, the 5:1 column is nearly one and half times that of the 20:1 column at |0.12| m s^{-1}. There is very little difference between the two reaction rates for the time-averaged curves; nevertheless there is a slight asymmetry for growth rate A.

Figure 4 depicts the profiles for the volume fraction of the gas and solid phases. The profiles for both phases display the plug flow form that was observed with the equivalent models for gas-liquid and gas-liquid-solid flows[1-2]. The increase in the gas fraction that occurs in the centre of the column corresponds to a slight decrease in the solid fraction. Yet higher up the column the influence of each discrete phase over the other is not as distinct, as much lower fractions are observed for both phases. The profiles of the phase fractions and the vertical velocity indicate that there is a small influence of the growth rate on the overall hydrodynamics of the bubble column compared with the overall impact that the solid phase has in reducing the velocity and gas fractions observed. However, the tiny influence of the growth rate on the hydrodynamics and the solids fraction did not change the rate at which the substrate was consumed or the growth rate of the biomass. Although the yield coefficients for the product strongly influenced the amount of product formed, as indicated by the five fold increase observed for both points in the time series (Figure 2).

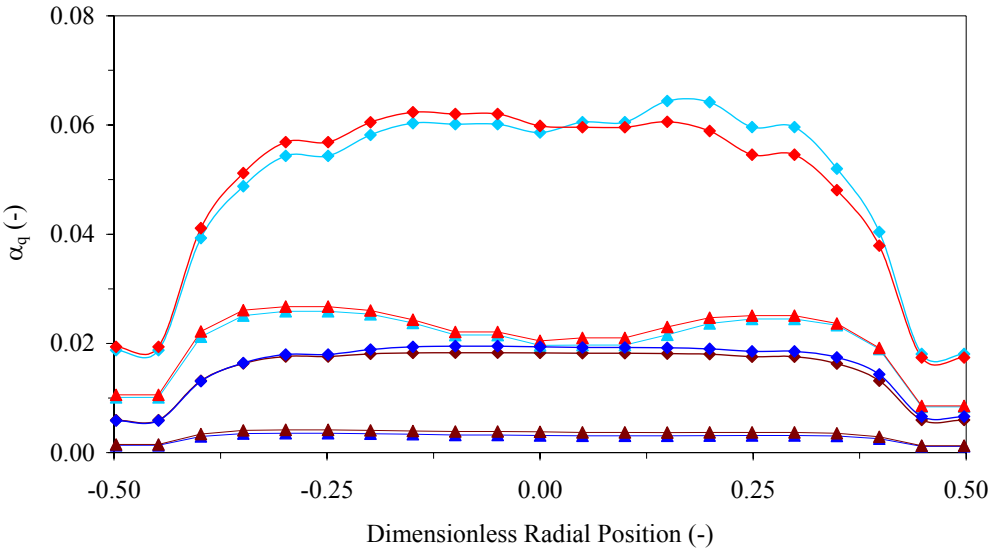

Figure 4. Profiles of volume fractions of the dispersed phases averaged with respect to time (-);Brighter colours at a height of 2.5 column diameters and darker colours at a height of 10 column diameters; Blue profiles for rate A and red profiles for rate B;

Figure 5 displays the velocity vector plots if the top and bottom half of the column for both growth rates. Note that only 1 of every 5 vectors is depicted here for reasons of clarity. This plot confirms that the intensity of the turbulence is increased in the lower half of the column. The effect of the growth rate on the vector fields at 200 seconds of simulated time shows that there are subtle differences to the vortical structure that result from local changes to the solids fraction caused by the different growth rates.

The contour plots of the biomass (Figure 6) and substrate concentrations (Figure 7) and product (Figure 8) are presented in a similar way to the vector plots in Figure 5. All the figures show an increase in the concentration at the top of the column where the intensity of the turbulence is not as significant. It is understandable that the local increase to the product concentration corresponds to the local increase in the biomass concentration; however this is also observed for the substrate. Therefore, the effect that the gas phase equation has on the local concentrations could be significant; this could be the result of the mixture formulation used to represent both the gas, liquid and solid phases.

If the distribution of the substrate is realistic, then strong concentration gradients for the substrate can be observed between vortical structures. Therefore, the environmental conditions that the biomass is exposed to in each vortex can be different. Thus, significant effects on the reaction kinetics of the biomass will be observed particularly in regions of low substrate concentration. However, this is dependent on how quickly the micro-organism is responds to the environment it is exposed to and the nature of the substrate considered (i.e. glucose, oxygen, trace elements).

This is particularly critical for aerobic processes where oxygen is the limiting substrate, as zones where the oxygen concentration is low or zero will severely impair the ability of the organism to grow and thus affect the product formation rate. Regions where the oxygen concentration is zero can be found in more complex reactors (i.e. airlift reactors, activated sludge oxidation ditches). These reactors have regions that can be some distance from the gas distributors, thus any gas found in these regions may be depleted of oxygen and the local concentration of oxygen may also be low as the biomass consumes all the dissolved oxygen.

For example of the influence of the local substrate concentration on the functional pathways of bacteria have been studied with the application of Activated Sludge Models (Henze et al., 2000) to local hydrodynamic models of oxidation ditches (Cartland Glover et al., 2005; Cartland Glover et al., 2005ABC;

Littleton et al., 2001; Littleton et al., 2003; Oda et al., 2005). These studies reported the influence that the local oxygen concentration has on the different biochemical reaction pathways that are utilised by the biomass present in such processes and the effect this had on the treatment regimes observed. Therefore, identification dead zone, regions where the interphase mass transfer is poor or where starvation of the biomass occurs due to a lack of the substrate is one of the key advantages of using CFD.

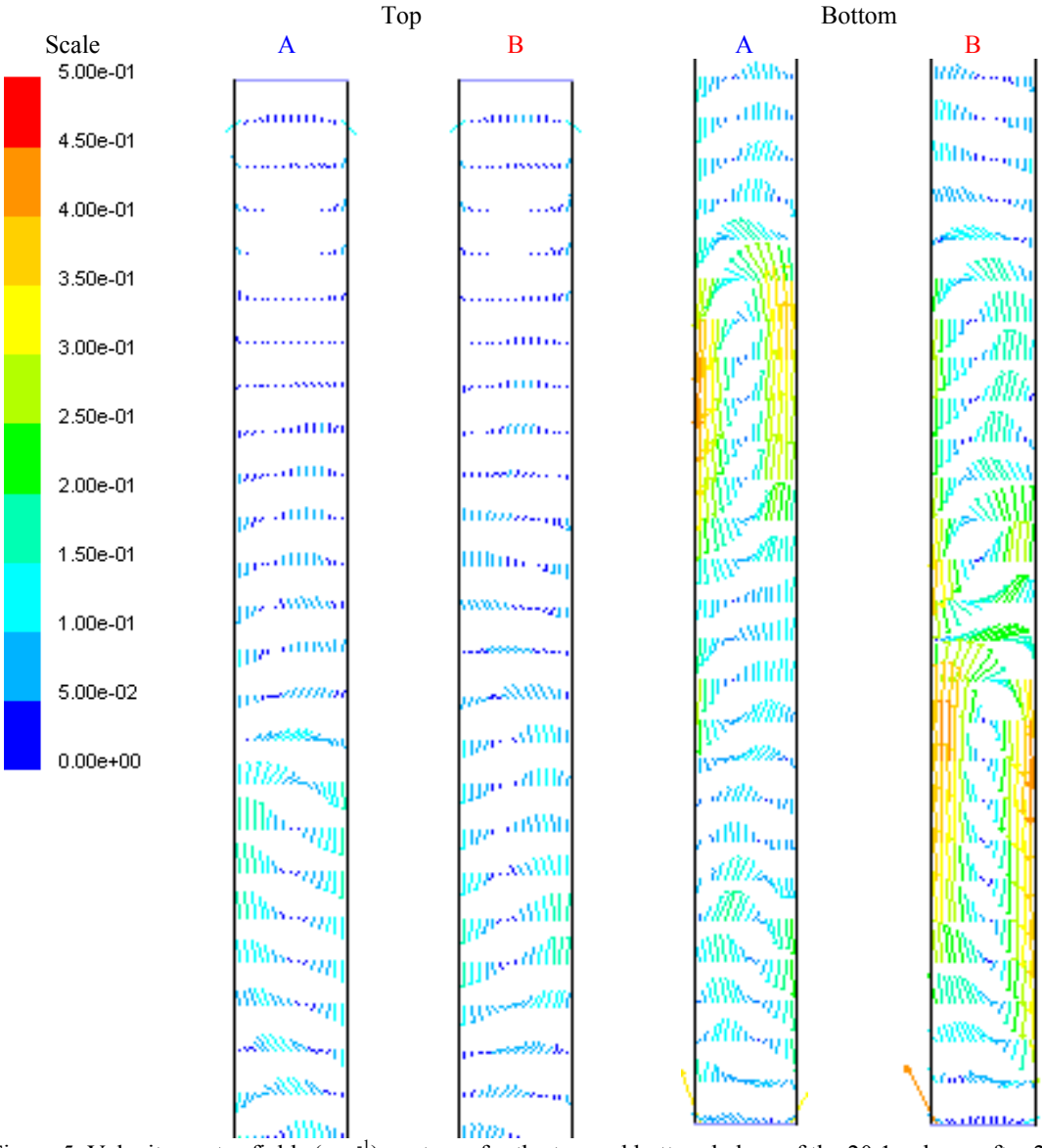

Figure 5. Velocity vector fields (m s^{-1}) contours for the top and bottom halves of the 20:1 column after 200 s at growth rates A and B

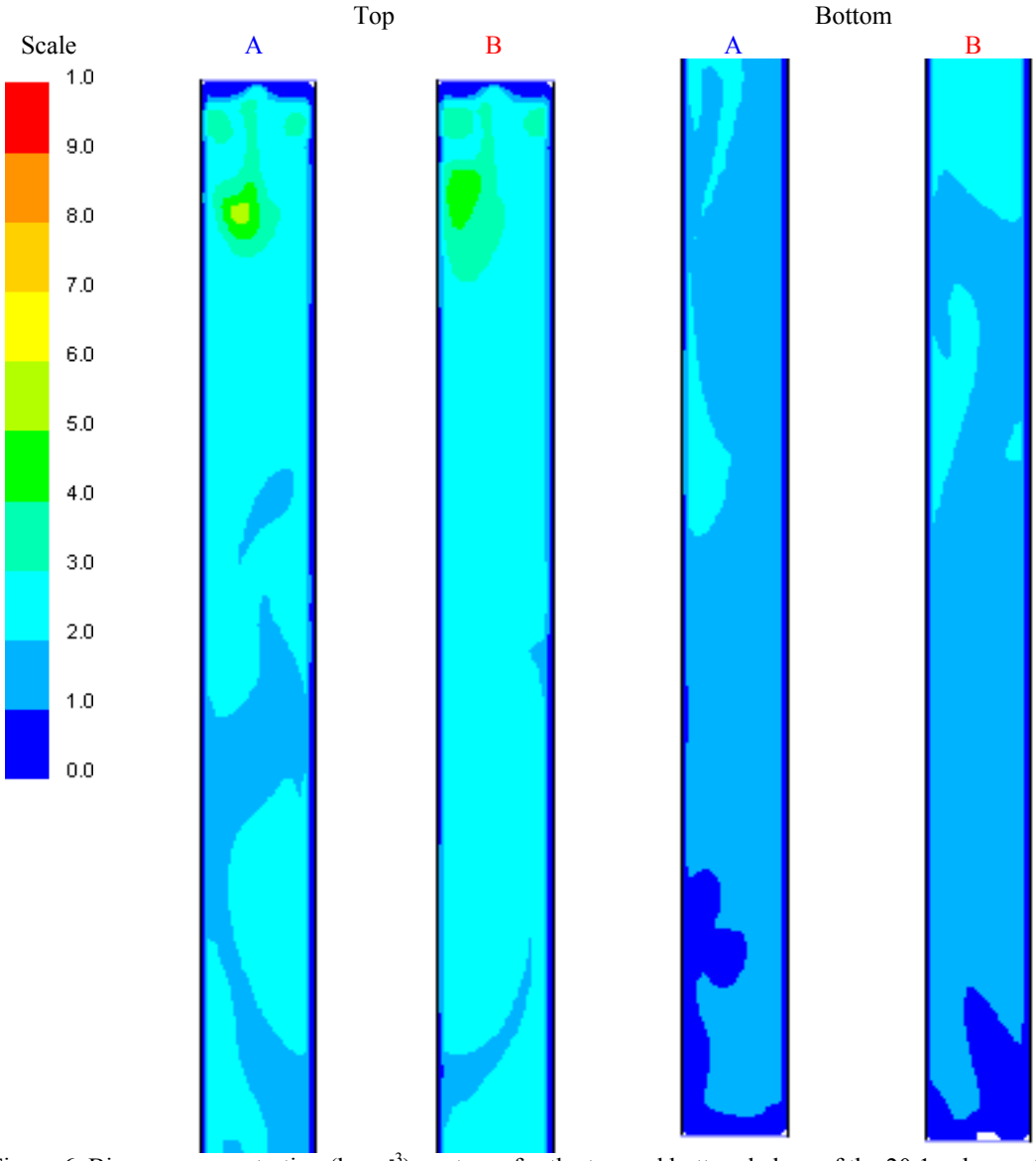

Figure 6. Biomass concentration (kg m^{-3}) contours for the top and bottom halves of the 20:1 column after 200 s at growth rates A and B

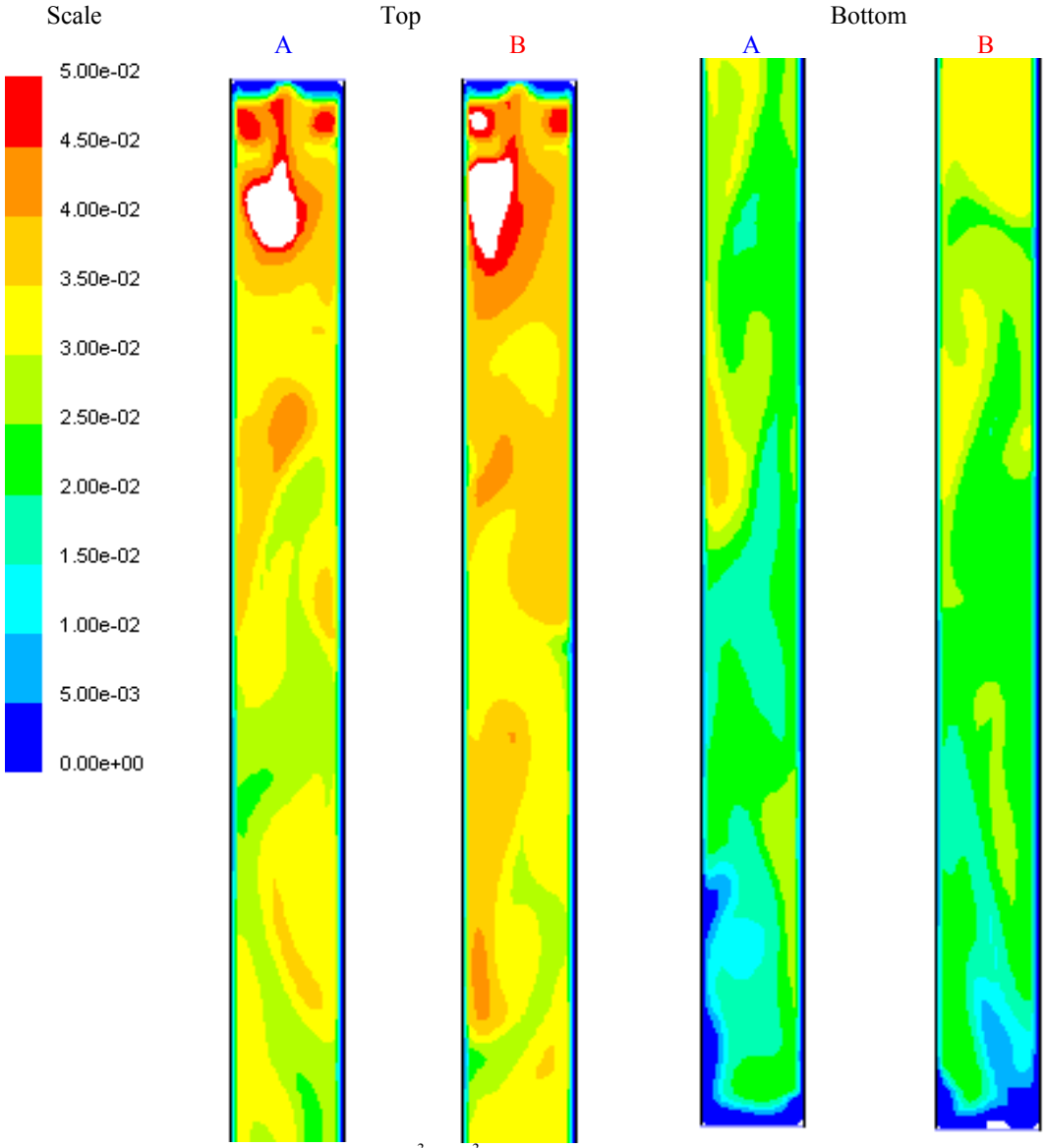

Figure 7. Substrate concentration (kg m^{-3})*10^3 contours for the top and bottom halves of the 20:1 column after 200 s at growth rates A and B; Note that the white region is where the substrate region exceeds the scale specified

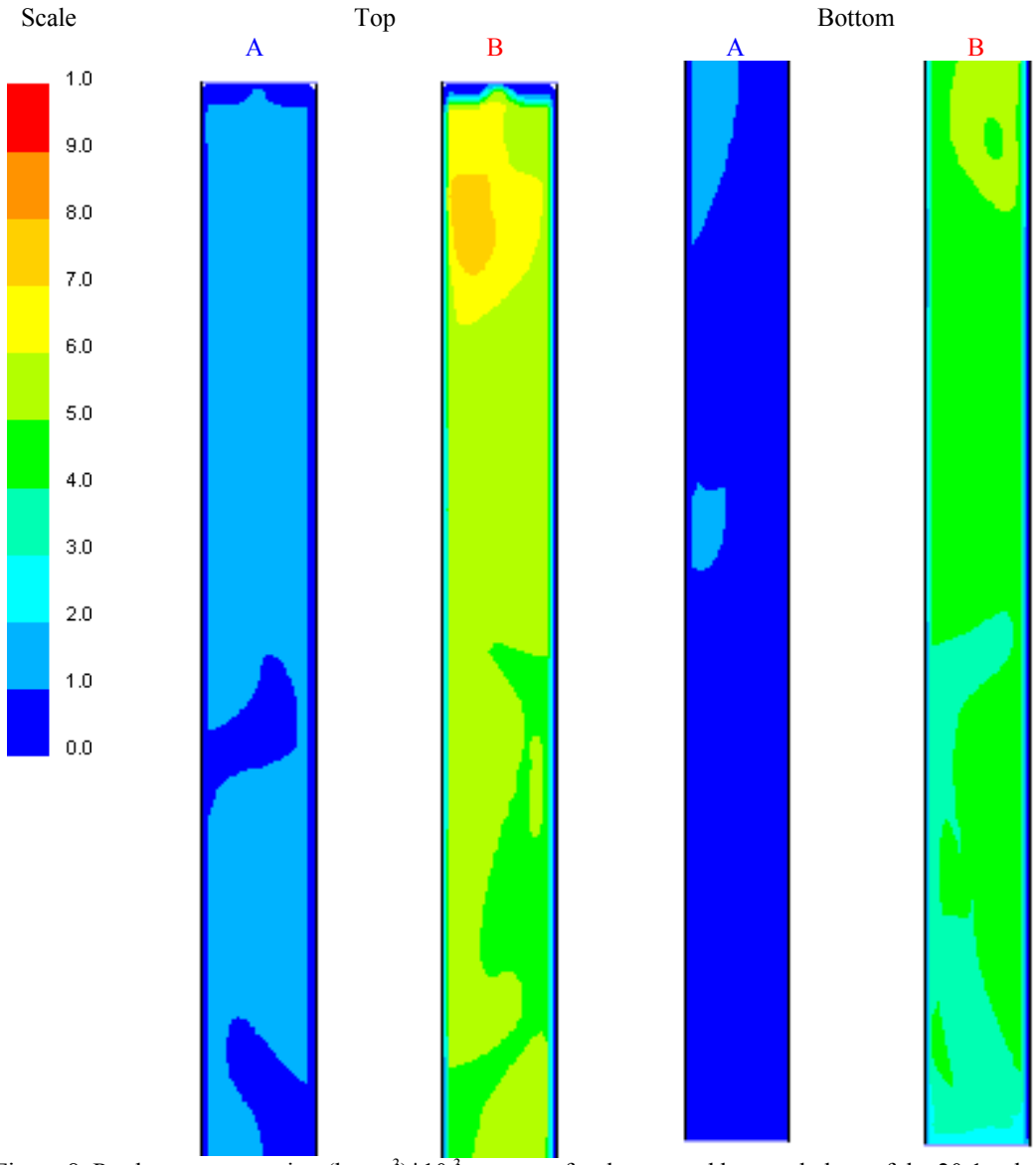

Figure 8. Product concentration (kg m^{-3})*10^{-3} contours for the top and bottom halves of the 20:1 column after 200 s at growth rates A and B

4. CONCLUSIONS

Biochemical reaction models were implemented with the gas-liquid-solid mixture model, utilising four scalar equations. The reactions mimicked processes that occur within a microbial culture quite well. Reaction rates from a strain of the mould *Aspergillus niger* were used to test the application of the reaction models. The flow structures that were produced were similar to the earlier gas-liquid and gas-liquid-solid flow cases (Cartland Glover et al., 2004A-B).

The consumption of a substrate displayed power law properties that have long been associated with fermentation of sugars by *Aspergillus niger* (Atkinson and Mavituna, 1983; Bailey and Ollis, 1986; Berovič et al., 1993; Chisti, 1989; ; Coulson et al., 1994; Deckwer, 1986; Finkelsein and Ball, 1991; Haq et al., 2002; Roehr et al., 1981; Sakurai et al., 1997; Sankpal et al., 2001). Yet the rate of consumption was

high for the length of the simulation considered (i.e. 200 seconds). This was probably due to defining the substrate in terms of concentration and the lack of diffusion models for transport through the pellets and across cell membranes. Other reasons could include how the yield coefficients and growth rates were defined, either in terms of the whole fermentation or for specific stages of the life cycle of the culture. The formation of a product also showed power law tendencies as the mass of the product increased, but this was at a much lower rate than was observed for the substrate consumption.

Improvements that need to be considered include modelling the transport of oxygen across the gas-liquid interface and the diffusion of chemical species into and out of the cell culture. Other aspects that are influential encompass effects such as the local shear rate and the local concentration of species display on the growth of the cell culture (i.e. trace metals, nitrogen, phosphorous and sulphur). Therefore, more detailed cell growth and maintenance models are required to examine the majority of the effects of the species in the culture broth. The impact that the shear rate had on the discrete phase flow phenomena and cell growth, included effects such as particle break-up, pellet formation and particle collisions. Therefore, to effectively model biochemical reactions it is essential to include the influence that shear rate displays on cell growth and pellet formation. Work on this and related matters is underway and will be reported elsewhere.

ACKNOWLEDGEMENTS

The models described in this paper formed part of a project funded by the EU through the INCO-COPERNICUS Grant (ERB IC15-CT98-0904). We are also grateful for Fluent Incorporated who provided the CFD code employed here.

NOMENCLATURE

d	particle diameter (m)
F	external forces (kg m s^{-2})
f	dimensionless friction factor (-)
g	acceleration due to gravity vector (0 –9.81 0 m s^{-2})
M	mass (kg)
p	pressure (N m^{-2})
Re	Reynolds number (-)
r	rate of reaction (kg m^{-3} s^{-1})
S	source term
t	time (s)
U	mean velocity (m s^{-1})
u	velocity component (m s^{-1})
V	volume (m^{-3})
v	slip velocity component (m s^{-1})
x	spatial co-ordinate (m)
Y	yield coefficient ((kg) $(kg)^{-1}$)

Mathematical operators

D	total differential operator
∂	partial differential operator
∇	del operator
Σ	summation
$\rightarrow$	vector form of variable (i.e. representing i, j and k forms of the variable as a matrix)
$\bar{}$	bar denoting an averaged product

Greek symbols

β	coefficient of thermal expansion (K^{-1})
δ	Kronecker symbol
ε	rate of dissipation of turbulent energy ($m^2\ s^{-2}$)
ϕ'	volume fraction (-)
ϕ''	concentration (kg m^{-3})
Γ	diffusion coefficient for the scalar function (m^2)
λ	specific growth rate (s^{-1})
μ	dynamic viscosity (kg $m^{-1}\ s^{-1}$)
θ	temperature (K)
ρ	density (kg m^{-3})
Ω	mean rate of rotation tensor

Subscripts and superscripts

A	substrate or molasses species
B	biomass species
C	product or citric acid species
CC	computational cell/reactor volume
c	continuous phase
DG	gas phase drift velocity
DS	solid phase drift velocity
Dq	drift velocity of the qth phase
eff	effective value in reference to the addition of turbulent and non-turbulent contributions of a variable
G	gas phase
i	co-ordinate index
j	co-ordinate index normal to i
L	liquid phase
l	co-ordinate index
m	co-ordinate index
mp	mixture phase index
n	number of phases
q	discrete or particulate phase (including bubbles, drops and particles)
qm	maximum discrete phase fraction (i.e. 0.62 for solids and 1 for bubbles)
r	phase index
S	solid phase volume fraction
SG	parameter where the concentration, mass or volume is increased by cell growth
s	mass source for the conservation of mass
ϕ'	diffusion coefficient of the volume fraction equations, 0.1
ϕ''	diffusion coefficient of the concentration equations, 0.001
*	viscosity power function, different for solid and gas phases

REFERENCES

Alvarez-Vasquez, F., González-Alcón, C. and Torres, N. V., "Metabolism of citric acid production by Aspergillus niger: Model definition, steady-state analysis and constrained optimisation of citric acid production rate", Biotechnol. Bioeng., Vol. 70, No. 1, 82-108 (2000).

Atkinson, K. and Mavituna, F., "Biochemical Engineering and Biotechnology Macmillan", UK (1983).

Bailey, J. E. and Ollis, D. F., "Biochemical Engineering Fundamentals", McGraw-Hill, London, (1986).

Berovič, M., Koloini, T., Olsvik, E. S. and Kristiansen, B., "Rheological and morphological properties of submerged citric acid fermentation in stirred tank and bubble column reactors", Chem. Eng. J. and Biochem. Eng. J., Vol. 53 No. 2 B35-B40 (1993).

Cartland Glover, G. M., "The use of computational fluid dynamics in the design of bubble column reactors", PhD Thesis, Aston University, UK (2002).

Cartland Glover, G. M., and Generalis, S. C., "The modelling of buoyancy driven flow in bubble columns", Chem. Eng. Processing, Vol. 43, No. 2, 101-115 (2004A).

Cartland Glover, G. M., and Generalis, S. C., "Gas-liquid-solid flow modelling in a bubble column", Chem. Eng. Processing, Vol. 43, No. 2, 117-126 (2004B).

Cartland Glover, G.M., Printemps, C.P., Essemiani, K., Meinhold, J., "Modelling of wastewater treatment plants – How far shall we go with sophisticated modelling tools?" In: Proceedings of the IWA Conference on Leading Edge Technologies, Sapporo, Japan, (2005).

Cartland Glover, G. M., Vermande, S., Essemiani, K., Meinhold, J., "Using global and local modelling tools to simulate biochemical reactions in a Sequential Batch Reactor", In: Proceedings of the 7th International Conference on Gas Liquid and Gas Liquid Solid Reactor Engineering, Strasbourg, France, (2005A).

Cartland Glover, G. M.,Vermande, S., Essemiani, K., Meinhold, J., "A dual approach to the hydrodynamic and biological modelling of Activated Sludge Basin", In Review (2005B).

Cartland Glover, G. M., Vermande, S., Essemiani, K., Meinhold, J., "Predicting the effect of mixing on oxygen transfer and nutrient removal in Activated Sludge Basins", In: Proceedings of the AIChE Annual Meeting 2005, Cincinnati, USA (2005C).

Chisti, M. Y., "Airlift Bioreactors", Elsevier, London, (1989).

Coulson, J. M., Richardson, J. F. and Peacock, D. G., "Chemical Engineering Volume 3" Elsevier, Oxford (1994).

Deckwer, W. -D., "Bubble Column Reactors", Wiley, Chichester, (1992).

Finkelstein, D. B. and Ball, C., "Biotechnology of filamentous fungi: technology and products", Butterworth-Heinemann, Massachusetts (1991).

Fluent Incorporated, "FLUENT 5 Users Guide", Fluent Incorporated, Lebanon, New Hampshire (1998).

Haq, I. -U., Ali, S., Qadeer, M. A. and Iqbal, J., "Effect of copper ions on mould morphology and citric acid productivity by Aspergillus niger using molasses based media", Process Biochem., Vol. 37, No. 10, 1085-1090 (2002).

Henze, M., Gujer, W., Mino, T., van Loosdrecht, M., "Activate sludge models ASM1, ASM2, ASM2d ASM3", Scientific and Technical Report No. 9, IWA Publishing, London, (2000).

Ishii, M. and Zuber, N., "Drag coefficient and relative velocity in bubbly, droplet and particulate flow", AIChE J Vol. 25, No. 5, 843-854 (1979).

Ishii, M. and Mishima, K., "Two-fluid model and hydrodynamic constitutive relations", Nucl. Eng. Des. Vol. 82 No. 2-3, 107-126, (1984).

Kissel, J. C., McCarty, P. L. and Street, R. L., "Numerical simulation of mixed-culture biofilm", J Environ. Eng. Vol. 110, No. 2, 393-411 (1984).

Littleton, H.X., Daigger, G.T., Strom, P.F., Application of computational fluid dynamics to closed loop bioreactors. In: Proceedings of WEFTEC 2001, Atlanta, Georgia, USA, (2001).

Littleton, H.X., Daigger, G.T., Strom, P.F., Cowan, R.A., "Simultaneous biological nutrient removal: evaluation of autotrophic denitrification, heterotrophic nitrification and biological removal in full-scale systems", Water Environ. Res., Vol. 75 No. 2, 138-150, (2003).

Manninen, M., Taivassalo V. and Kallio, S., "On the mixture model for multiphase flow", VTT Publications, Finland (1996).

Oda, T., Yano, T., Niboshi, Y., "Development and exploitation of a multipurpose CFD tool for optimisation of microbial reaction and sludge flow", In: Proceedings of the Leading Edge Treatment Technologies Conference, Sapporo, Japan, (2005).

Rittmann, B. E. and McCarty, P. L., "Model of steady-state-biofilm kinetics", Biotechnol. Bioeng. Vol. 22, No. 11, 2343-2357 (1980).

Roehr, M., Zehentgruber, O. and Kubicek, C. P., "Kinetics of biomass formation and citric acid production by Aspergillus niger on pilot plant scale", Biotechnol. Bioeng., Vol. 23 No. 11, 2433-2445 (1981).

Sakurai, A., Imai, H., Takenaka, Y. and Sakakibara, M., "Simulation of citric acid production by rotating disk contactor", Biotechnol. Bioeng., Vol. 56, No. 6, 689-696 (1997).

Sankpal, N. V., Joshi, A. P. and Kulkarni, B. D., "Citric acid production by Aspergillus niger immobilized on cellulose microfibrils: influence of morphology and fermenter conditions on productivity", Process Biochemistry, Vol. 36 No. 4, 1129-1139 (2001).

Sanyal, J., Vásquez, S., Roy, S. and Dudukovic, M. P., "Numerical simulation of gas-liquid dynamics in cylindrical bubble column reactors", Chem. Eng. Sci. Vol. 54, No. 21-22, 5071-5083, (1999).

Sinclair, C. G. and Kristiansen, B., Ed by J. D. Bu'Lock, "Fermentation kinetics and modelling", Open University Press, Milton Keynes, (1987).

Wanner, O. and Gujer, W., "A multispecies biofilm model", Biotechnol. Bioeng., Vol. 28 No. 3, 314-328 (1986).

Wood, B.D. and Whitaker, S., "Diffusion and reaction in biofilms", Chem. Eng. Sci., Vol. 53, No. 3, 397-425 (1998).

Zuber, N. and Findlay, J. A., "Average volumetric concentrations in two-phase flow systems", J Heat Trans. Vol. 87, No. 4, 453-468 (1965).